29-state R-matrix investigation of resonances in e^--He scattering at low energies: $1\,^1S-3\,^{3,1}S$ and $1\,^1S-4\,^{3,1}S$ excitation cross sections

W. C. Fon, K. P. Lim,* and K. Ratnavelu
Department of Mathematics, University of Malaya, 59100 Kuala Lumpur, Malaysia

P. M. J. Sawey
Department of Applied Mathematics and Theoretical Physics, The Queen's University, Belfast BT7 1NN, Northern Ireland
(Received 8 November 1993; revised manuscript received 8 August 1994)

The 29-state R-matrix calculations in which physical target states of helium with $n=1$, 2, 3, 4, and 5 are included in the total scattering wave functions have been employed by Fon, Lim, and Sawey [J. Phys. B **26**, 305 (1993)] to obtain the cross sections for the electron-impact excitations of the $2\,^{3,1}S$ states of helium. The same R-matrix calculations are now extended to obtain integral and differential cross sections of $1\,^1S-3\,^{3,1}S$ and $1\,^1S-4\,^{3,1}S$ transitions. The calculations are performed at 400 energies ranging from the thresholds to 24.1 eV. The results, together with those of Fon, Lim, and Sawey for $n=2$ excitation, are used to analyze the experiments of Allan [J. Phys. B **25**, 1559 (1992)]; his interpretation of the decay of the doubly excited Wannier-ridge resonances is reexamined.

PACS number(s): 34.80.Dp, 03.65.Nk

I. INTRODUCTION

The classical Wannier theory (Wannier [1], Vinkalus and Gailitis [2]) suggests that, in the electron-atom ionization process at threshold, the two outgoing electrons leave the atomic nucleus diametrically at 180° and that the excess energy is almost uniformly shared by the outgoing electrons. This was verified experimentally by Cvejanovic and Read [3]. Allan [4] reported measurements of the electron-impact differential excitation cross sections for the $n=2$, 3, $4\,^3S$, and $5\,^3S$ excitation of helium from the ground state at energies ranging from the threshold to 24.1 eV. By examining the profile of these excitation functions, he found evidence to suggest that the energy partition between the two electrons of doubly excited Wannier-ridge states appeared to be uniform, with all possible combinations of the bound- and the free-electron energies having equal weights. This behavior resembles the nearly uniform energy partition between the two escaping electrons of a ridge state above the ionization threshold. Theoretically, the threshold behavior of the ionization process as described by the Wannier theory is basically classical, while the decay of the doubly excited Wannier-ridge resonances at energies significantly below the ionization threshold is quantum mechanical in nature. If the observation of Allan [4] were to be correct, this could have serious implications in our understanding of the nature of Wannier-ridge resonances. This might suggest that the electron-electron correlation and interchannel coupling is so dominant as to give rise to classical formation of a highly symmetrical localized electron-density distribution along the Wannier ridge.

Experimentally, Allan's measurement [4] is a very difficult experiment to perform, and the findings must be verified and confirmed. Although Pichou *et al.* [5] had reported earlier absolute measurements on the inelastic differential cross sections for the $n=2$ and $3\,^3S$ states of helium at the same energy range under consideration, the measurements for the $1\,^1S-3\,^3S$ differential cross sections with general accuracy cited to be around ±40% and electron energy resolution of 55 meV, at best, only represent a fuzzy average of the actual excitation functions. The experimental difficulties in the measurements of the differential cross sections to the $n\geq 3$ states of He lie in the facts that (1) the cross sections to these states are generally smaller than those of $n=2$ excitations by an order of magnitude, (2) the differences in energy levels within the various states of $n\geq 3$ are very much narrower than those of $n=2$, and (3) there is a greater abundance of resonances observed at the vicinity of the thresholds for $n\geq 3$. As a result, the extraction of information on resonant parameters (e.g, position, width, symmetry, and mode of decay) from the profile of the excitation function is much more difficult. It is further complicated by the fact that, at these energies, the cross sections of the manifolds of the same n are likely to be equally significant relative to each other, and experimentally it is extremely difficult to resolve these states.

In this paper, the R-matrix calculations of Berrington and Kingston [6] (19-state) and Sawey *et al.* [7] (29-state) have been employed to provide theoretical verification of the findings of Allan [4]. The work described here is part of a continuing effort to study resonances in electron scattering from helium at low energies and follows from the works of Fon, Lim, and Sawey [8,9].

*Permanent address: MARA Institute of Technology, 40450 Shah Alam, Selangor, Malaysia.

II. R-MATRIX CALCULATION

The R-matrix method of electron-atom collision has been discussed in detail by Burke, Hibbert, and Robb [10]. The collision calculations are carried out in LS coupling using the R-matrix computer package of Berrington *et al.* [11]. The target wave functions, oscillator strengths, and energy levels used in this calculation have already been described in full by Berrington and Kingston [6] and Sawey *et al.* [7]. However, to recapitulate, the wave function describing the three-electron scattering systems can be expanded as

$$\Psi_k = \mathcal{A} \sum_{ij} a_{ijk} \Phi_i u_j(r) + \sum_j b_{jk} \phi_j \ , \tag{1}$$

where Φ_i are the channel functions formed from the target states of the two-electron system, the u_j are the radial basis functions describing the motion of the scattered electron, and ϕ_j are the three-electron functions which allow for short-range correlation effects and completeness. These three electron-bound terms are also designed to represent the target states of the singly ionized atom, coupled to two bound electrons simulating the possible formation of three-electron resonances.

In theory, if the summation in (1) included all the bound states of helium exactly and also included integration over the continuum states of helium, then the results would be exact. However, in practice, we can only include a small number of target states in (1). Only the lowest 19 ($n=1$, 2, 3, and 4) and 29 ($n=1$, 2, 3, 4, and 5) states of helium have been respectively included in the R-matrix calculations presented here. The introduction of the highly excited $n=5$ levels for the 29-state calculation necessitates the increase of the R-matrix radius to 83 atomic units (a.u.) compared with 60 a.u. for the 19-state calculation. Forty-eight continuum terms are required for each channel, and the maximum number of coupled channels rises to 69. The largest Hamiltonian matrix that must be diagonalized is of the order 3363. The partial waves included in the 19-state calculation are $L=0$ to 9, while only partial waves of $L=0$ to 4 are included in the 29-state calculations. Although we did not allow for ionization channels, we do not expect that the continuum effects are important enough to affect the accuracy of our calculation significantly in the energy range from the $3\,^3S$ threshold to 24.1 eV, in which all the ionization channels are closed and only a few discrete channels are open. The scattering processes are predominated by resonances.

III. RESULTS AND DISCUSSION

The 19-state and 29-state R-matrix calculations [6,7] have been extended to obtain the integral and differential cross sections for the following transitions:

$$e^- + \mathrm{He}(1\,^1S) \rightarrow e^- + \mathrm{He}^*(n\,^{3,1}S) \ , \tag{2}$$

where $n=2$, 3, and 4, at 650 and 400 energies respectively from the thresholds to 24.1 eV. The differential cross sections are computed at scattering angles $\theta=20°$, 30°, 55°, 60°, 90°, 120°, 125° and 140°.

A complete presentation of the results of these calculations would require publication of a very large table giving the cross sections as functions of several hundred energies. This is impractical. Therefore, it has been decided to present here some illustrative results in graphic form. However, a complete numerical table of the results by energies at respective fixed angles can be obtained on request from the authors [12].

In presenting the R-matrix calculations, a small amount of energy ΔE is subtracted from the $1\,^1S$ ground state so as to reproduce the observed $1\,^1S-2\,^3S$ splitting of 19.82 eV. Subsequently, all the other thresholds and resonant positions are calibrated relative to the $2\,^3S$ threshold. Although the resulting computing threshold values are in good agreement with experiments of Martin [13], this does not mean that the computed thresholds are now in "exact" agreement with the energy spectra of Pichou *et al.* [5] and Allan [4], which, in fact, are not exactly in agreement among themselves. For the R-matrix calculations, each new target state introduced into the calculation brings with it a new series of energy levels and Feshbach resonances at impact electron energies below its threshold. This means that the energy spectra of the 19-state calculation are not exactly the same as those of the 29-state calculation. Appreciable displacements show up between the two scales when they are superimposed onto one another, and one of the curves appears to have been shifted away from the other. Especially over $n=3$, 4, and 5 excitation thresholds, where energy splitting is very narrow, the difference can become significant when the energy range is enlarged for detailed scrutiny. This was highlighted by Fon, Ratnavelu, and Sawey [14]. One of the ways to overcome this is to adopt the practice of "parallel" comparison as employed by Fon and Lim [15,16].

A. Integral cross sections for $1\,^1S-3\,^{3,1}S$ and $1\,^1S-4\,^{3,1}S$ excitations

Berrington and Kingston [6] suggest that close-coupling calculations for e-He scattering at low energies in which physical states with increasing principal quantum number n are used yield accurate excitation cross sections in the energy up to the highest threshold explicitly included, and that, at higher energies, the accuracy of the calculated excitation cross sections leaving the atom in a final state of principal quantum number n depends critically on the inclusion of target states with principal quantum number $n+1$ in the total wave-function expansion. For these reasons, the 11-state calculations are not included in the convergence studies in the $1\,^1S-n\,^{3,1}S$ (for $n \geq 3$) excitation cross section, and the 19-state calculations are not compared with the 29-state calculations for the $1\,^1S-4\,^{3,1}S$ excitation cross sections.

The 19-state and 29-state calculations on the integral cross sections of $1\,^1S-3\,^{3,1}S$ excitations are compared in Figs. 1(a) and 1(b) by superimposing the two R-matrix calculations onto each other. There is generally good agreement between the two R-matrix calculations; however, minor details differ. There are two notable differences: (i) The 19-state seems to have been shifted to the right of the 29-state as the incident energy converges

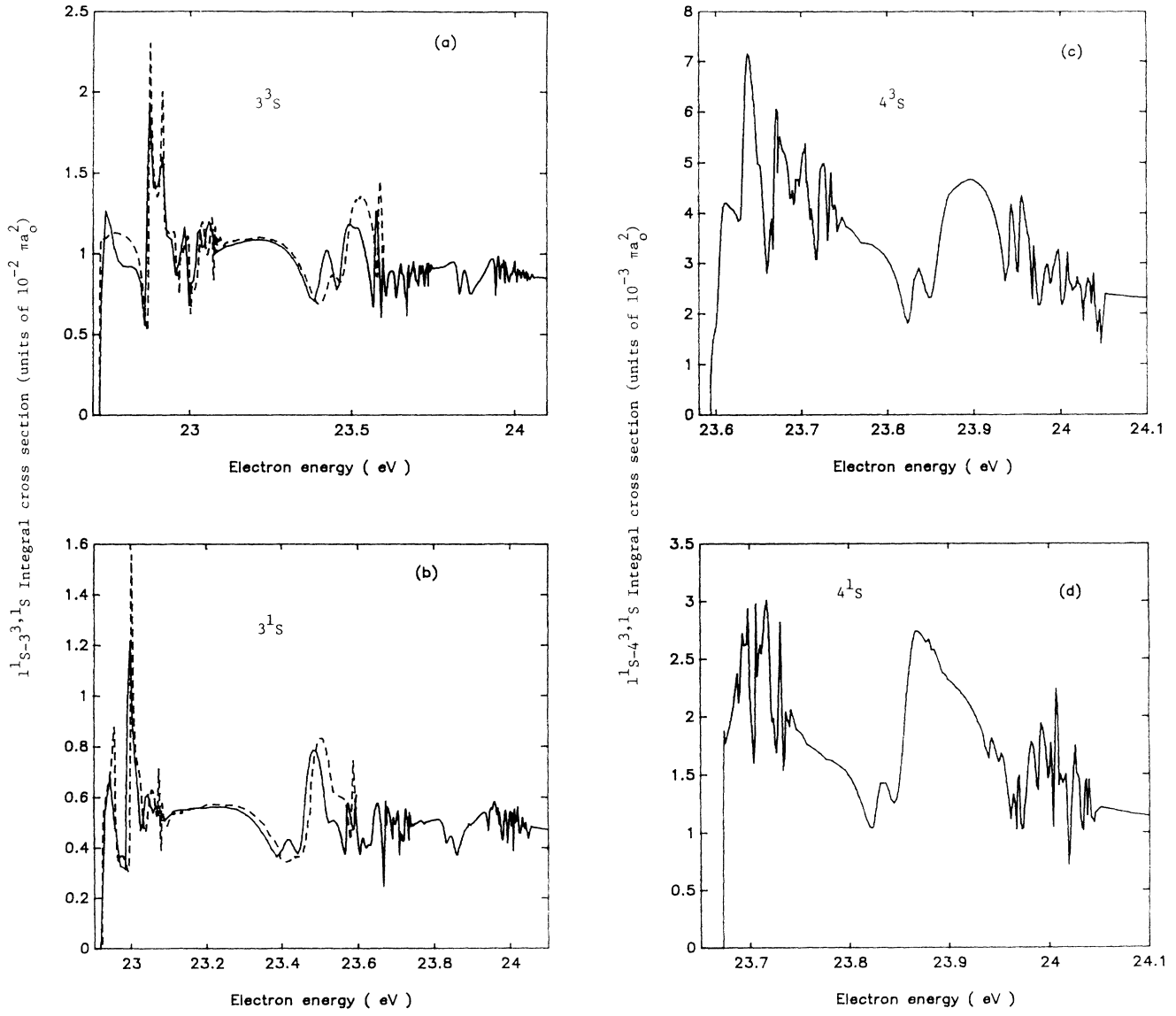

FIG. 1. Comparison between the 19-state and 29-state R-matrix calculations on $1\,^1S-3\,^{3,1}S$ and $1\,^1S-4\,^{3,1}S$ integral cross sections (units of πa_0^2). (a) $1\,^1S-3\,^3S$ excitation; (b) $1\,^1S-3\,^1S$ excitation; (c) $1\,^1S-4\,^3S$ excitation; (d) $1\,^1S-4\,^1S$ excitation. ——, the 29-state R-matrix calculation; — — —, the 19-state R-matrix calculation.

to the $n=4$ threshold. This is the direct consequence of the differences in the energy spectra between the 19-state and the 29-state calculations. The energy levels of the 29-state calculation, being more accurate, are systematically lower than the corresponding energy levels of the 19-state one; (ii) the qualitative shape of the 19-state calculation for the $1\,^1S-3\,^3S$ cross sections differs significantly from those of the 29-state calculation at energies just above the $3\,^3S$ threshold. This is due to the broad resonances $^2F^0$ and $^2D^e$ at energies 22.849 and 22.865 with widths of 53 and 37 meV respectively, which interact with the $3\,^3S$ threshold [see Fig. 1(a)]. Whenever a situation like this occurs, the convergence of the R-matrix calculations becomes a little slower (see Fon and Lim [17]).

Figures 1(c)–1(d) show only the 29-state calculations on the $1\,^1S-4\,^{3,1}S$ integral cross sections. There are no other theoretical calculations nor experimental measurements available for comparison, and the 19-state calculations are not expected to be too reliable here.

B. Differential cross sections for $1\,^1S-3\,^{3,1}S$ and $1\,^1S-4\,^{3,1}S$ excitations

Figures 2 and 3 compare the 29-state calculations on $1\,^1S-3\,^{3,1}S$ differential cross sections (DCS) (as functions of electron energies) with the experiments of Allan [4] at scattering angles of 20°, 60°, 90°, and 120°. On the whole, there is a general agreement in shape between the experiments and the theory, allowing for the fact that an energy

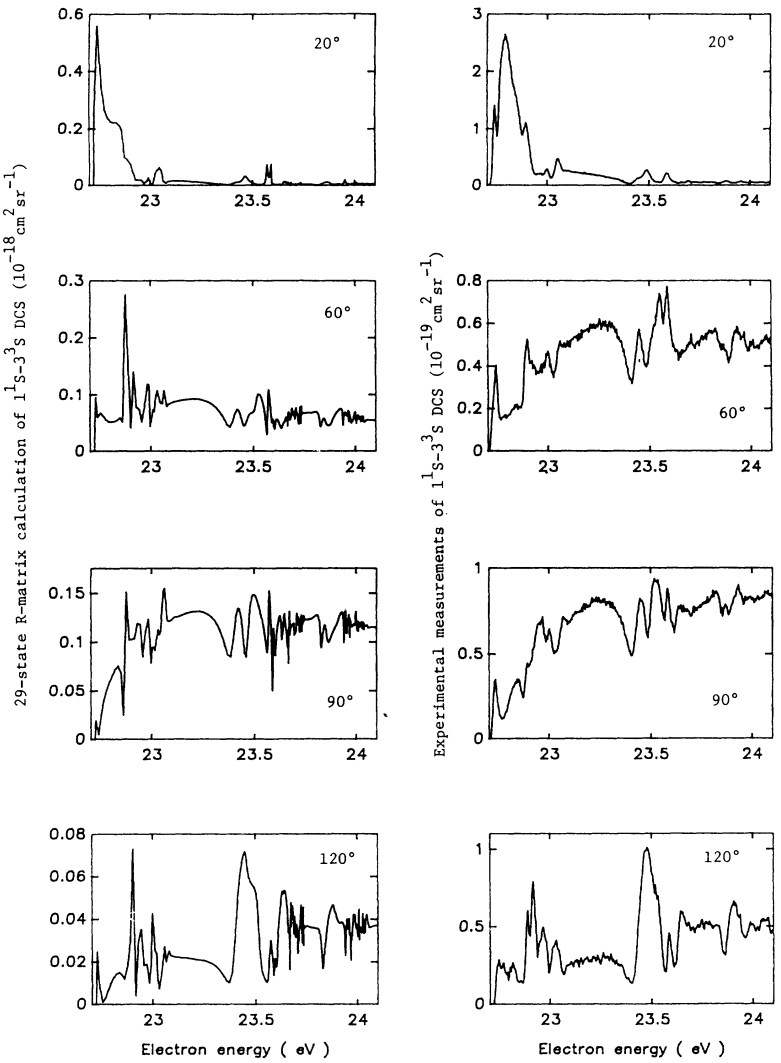

FIG. 2. Comparison between the 29-state results (left) and the experiments of Allan [4] (right) on the differential cross sections (10^{-18} $cm^2\,sr^{-1}$) for $1\,^1S-3\,^3S$ excitation of helium by electron impact at scattering angles of 20°, 60°, 90°, and 120°.

range of 1 eV has been enlarged in size to permit close scrutiny (see also Figs. 1 and 2 of [14]). However, appreciable discrepancy *does* exist in the detailed structure of the resonant profiles, especially at scattering angles of 60° for the $3\,^3S$ and 90° for the $3\,^1S$ excitation functions. At the proximity of the threshold, the difference could have been in part due to the threshold uncertainty mentioned by Phillips and Wong [18] and Pichou *et al.* [5]. On the other hand, sharp and narrow features appearing in the theoretical curves are not expected to be observed in the experimental excitation functions. This is due to limitation of the instrumental sensitivity and electron-beam resolution. Direct matching of the theoretical calculation with the experiments can be facilitated through the convolution procedure in which the 29-state results on differential cross sections are convoluted with a Gaussian of approximately 20 meV full width at half maximum to simulate the broadening of the finite resolution of the electron beam used in the experiments of Allan [4]. The convoluted 29-state *R*-matrix calculations on $1\,^1S-3\,^{3,1}S$ DCS at 120° and 90°, respectively, are now superimposed on the experiments of Allan [4] in Fig. 4, revealing reasonably good detailed agreement in the shape of the resonant features at energies away from the thresholds. However, the agreement on resonant positions and the underlying magnitudes is not so good. The positions of the resonances of the calculation appear to have been shifted slightly to the right of the experiments. In our preliminary report [14] we attributed this to the small difference in energy spectra between the computation and measurements. When two slightly different scales are superimposed onto one another, appreciable displacements show up, resulting in the shift of the theoretical curves away from the experiments. However, the discrepancy in magnitude cannot be easily explained (see [14]). This could not have been due to the fact that only a limited number of partial waves (from $L=0$ to 4) were taken into consideration in the 29-state calculation. At low energies, only a few partial waves are required to induce convergence on the calculation of DCS for the optical or spin-forbidden transitions like $1\,^1S-n\,^{3,1}S$. It was shown to be true for the $1\,^1S-2\,^{3,1}S$ excitation (see [9]). Figure 3

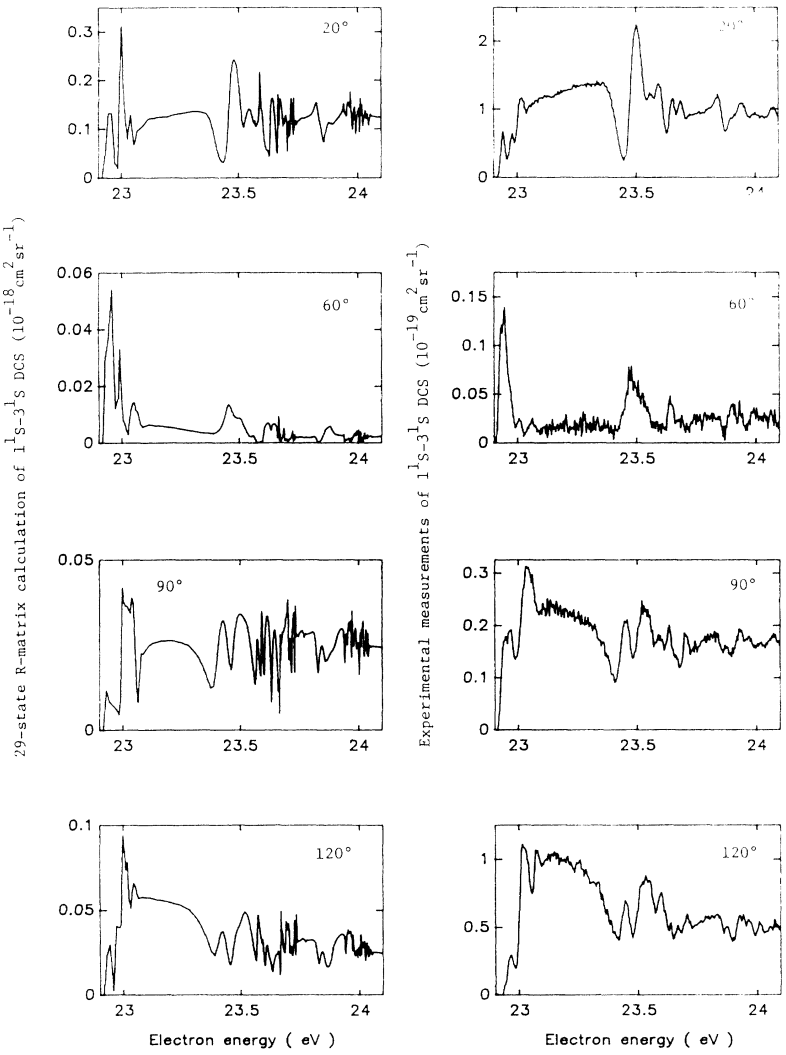

FIG. 3. Same as Fig. 2, except the comparison is now for $1\,^1S-3\,^1S$ excitation.

of our preliminary letter [14] shows excellent convergence in shape and magnitude between the 29-state and 19-state calculations on the DCS for the $1\,^1S-3\,^{3,1}S$ excitations at 23.22 eV, in which more partial waves (from $L=0$ to 9) were included in the 19-state calculation than that of the 29-state. The convergence is consistently reflected in Figs. 1(a) and 2(b) of [14] in the calculation of excitation functions for $1\,^1S-3\,^{3,1}S$ transitions. The convergence between the two R-matrix calculations implies that (i) inclusion of partial waves from $L=0$ to 4 is sufficient to achieve convergence for the 29-state calculation, and any discrepancy in shape and magnitude between the experiments and theories at angles greater than 20° is most unlikely, due to the neglect of higher partial waves (the contribution from the higher partial waves affects the scattering only at small angles); (ii) the Berrington-Kingston convergence rule holds for the calculation of $1\,^1S-3\,^{3,1}S$ differential cross sections. Further inclusion of target states of higher principal quantum number n should not significantly change the values of the DCS of $1\,^1S-3\,^{3,1}S$ excitations. Although this does not tell us anything about the contribution from the continuum states, at an energy range in which the physical mechanism is predominated by resonances, we would not expect the continuum effects to be significant here. However, this can only be determined by further theoretical investigations using the intermediate-energy R-matrix theory. Further experiments with higher electron-energy resolution and improved sensitivity would help to resolve the discrepancy.

The 29-state calculations on $1\,^1S-4\,^{3,1}S$ DCS are shown in Fig. 5 at scattering angles of 20°, 60°, 90°, and 120°. Comparison has not been attempted with the 19-state results for the same reason given in Sec. III A. While there are no experimental measurements on $1\,^1S-4\,^{3,1}S$ DCS, the electron-energy resolution of 20 meV may not be high enough to resolve the details of resonant profiles for the $1\,^1S-4\,^3S$ transition over an energy range of less than 0.5 eV.

C. Identification of resonances

Andrick [19] showed that Feshbach resonances lying just below the $3\,^3S$ threshold can be identified and posi-

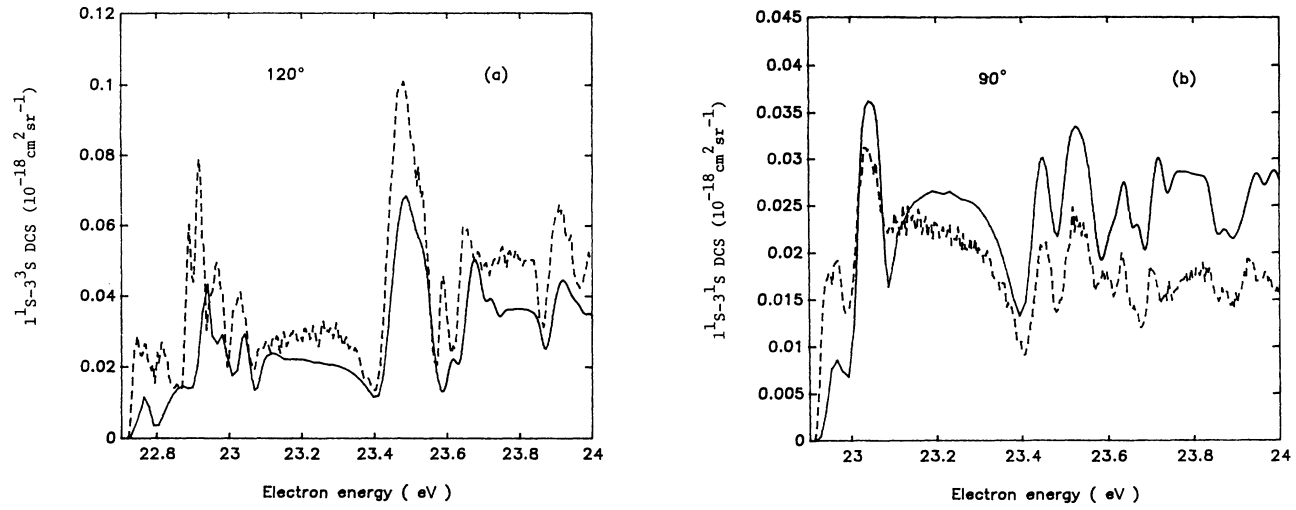

FIG. 4. Differential cross sections (10^{-18} cm^2 sr^{-1}) for electron-helium scattering as functions of electron energy. (a) $1\,^1S-3\,^3S$ excitation at 120°; (b) $1\,^1S-3\,^1S$ excitation at 90°. ——, the convoluted 29-state *R*-matrix calculations; — — —, the experiments of Allan [4].

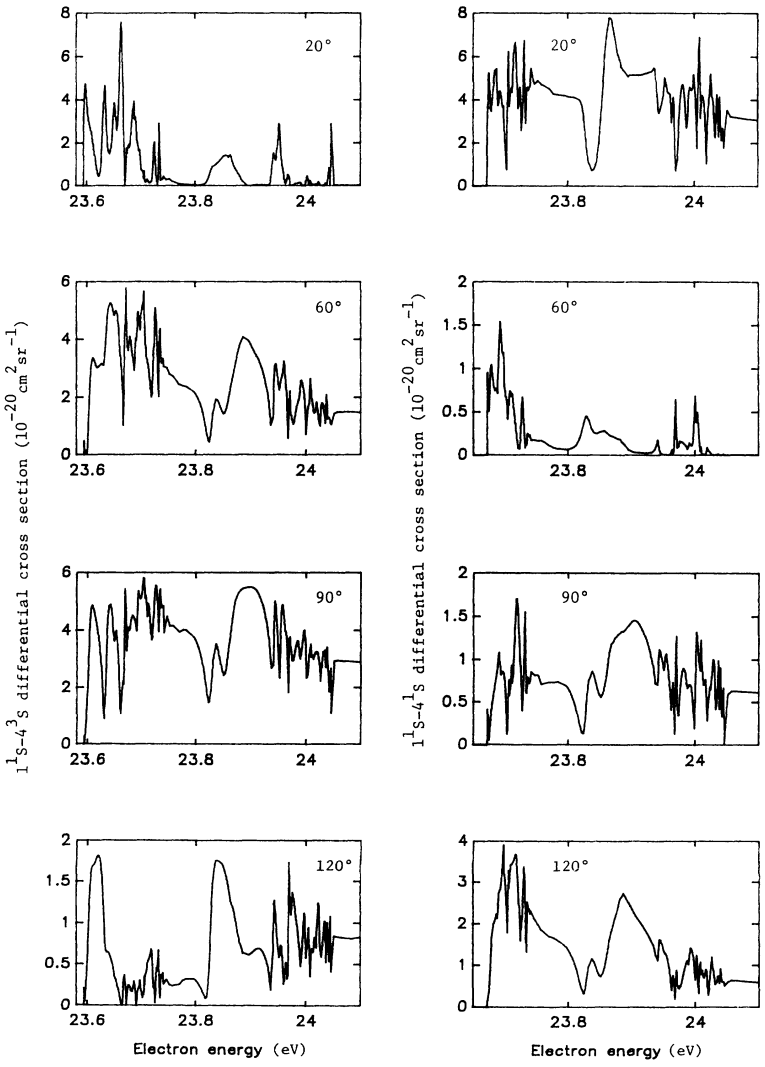

FIG. 5. The 29-state *R*-matrix calculations for $1\,^1S-4\,^{3,1}S$ differential cross sections (10^{-18} cm^2 sr^{-1}) at scattering angles of 20°, 60°, 90°, and 120°.

tions and widths extracted experimentally by measuring $1\,^1S-2\,^{3,1}S$ energy-dependent differential cross sections at suitable chosen scattering angles. This was confirmed by the 19-state R-matrix calculation of Fon and Lim [15]. However, no attempt was made to investigate resonances lying above the $3\,^3S$ threshold, where a greater abundance of resonances was found by Fon *et al.* [20]. As energy increases from the $3\,^3S$ threshold, investigation of resonances becomes further complicated by the following facts: (i) with the opening up of the $n=3$ excitation channels, the flux channeling into $1\,^1S-2\,^{3,1}S$ transitions is very much reduced and the size of the resonant features for the excitation functions becomes smaller; (ii) the relative simple structure of these excitations functions in this energy range does not reflect the richness of resonances reported by [20].

Figure 6 shows the profiles of the 19-state and 29-state

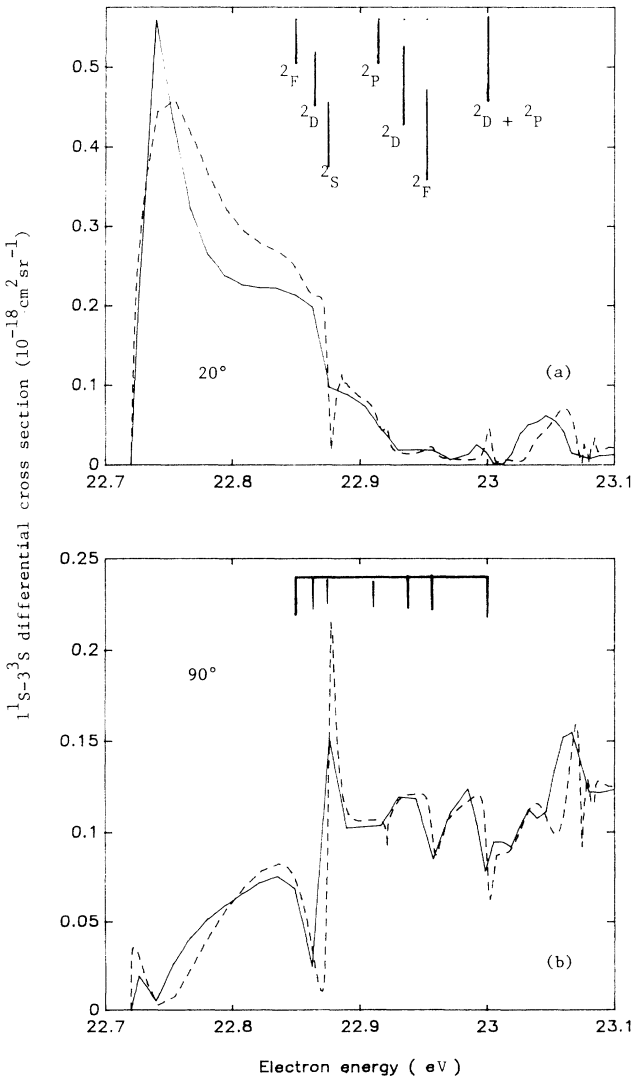

FIG. 6. The 19-state and 29-state R-matrix calculations of the $1\,^1S-3\,^3S$ differential cross sections (10^{-18} cm^2 sr^{-1}) as a function of incident electron energy at scattering angles (a) 20° and (b) 90°. The vertical bars represent the 19-state resonant positions of [20]. The curves are the same as Fig. 1.

R-matrix calculation of the $1\,^1S-3\,^3S$ DCS as a function of energy at scattering angles of (a) 20° and (b) 90°. We observe the following prominent features of the profiles shown in Fig. 6: (i) At a scattering angle of 20° [Fig. 6(a)], there is a distinct discrepancy between the two R-matrix calculations at energies lying immediately above the $3\,^3S$ threshold up to 22.85 eV. This is a general feature which shows up in almost all the scattering angles, with the exception of a few particular angles [see (ii)]. This gives rise to an outstanding discrepancy between the two R-matrix calculations on the integral cross section for the $1\,^1S-3\,^3S$ excitation, as discussed in Sec. III A [see Fig. 1(a)]. (ii) At the scattering angle of 90° [Fig. 6(b)], there is a distinct convergence of the two R-matrix calculations, even though a small energy range of 0.4 eV has been enlarged for detailed scrutiny. The contrasting behavior shown by the 90° profile actually confirms the suggestion that the discrepancy of the integral cross section in Fig. 1(a) is indeed due to broad resonances $^2F^o$ and $^2D^e$ at energies 22.849 and 22.865 eV, respectively, and to the $^2F^o$ resonance in particular, which is nearest the $3\,^3S$ threshold and has a width 53 meV. At the scattering angle of 90°, the dramatic effect caused by the $^2F^o$ resonance has been suppressed (see Fon and Lim [15]). However, at other angles, this effect can considerably slow down the convergence of the R-matrix calculation (see Fon and Lim [17]). (iii) To date, there are no reports on the 29-state calculation of resonant parameters, and in the absence of these parameters the 19-state resonant positions from Table 3 of [20] are represented as vertical bars in Fig. 6. Two notable facts are observed in Fig. 6(b): (a) The 29-state profile shifts to the left of those of the 19-state. This indicates that the resonance positions, if obtained by the 29-state calculation, would have to be systematically lower than those of the 19-state calculation; (b) it is clear that the relative simple structure of the $1\,^1S-3\,^3S$ profile in this energy range again does not reflect the richness of resonances reported in [20]. This implies that the $1\,^1S-n\,^{3,1}S$ DCS for $n=3$ and 4 do not improve the situation on the analysis of resonances due, to a large extent, to the narrow energy spacing and overlaps of resonances in this energy range.

D. The decay of doubly excited Wannier-ridge resonances

The present calculations on differential cross sections of the $1\,^1S-3\,^{3,1}S$ and $1\,^1S-4\,^{3,1}S$ transitions together with those of Fon, Lim, and Sawey [8,9] for $n=2$ excitations offer additional information on the role of the doubly excited Wannier-ridge resonances in different decay channels and their dependence on scattering angles.

Figure 7 compares resonant features of the $1\,^1S-n\,^{3,1}S$ ($n=2$, 3, and 4) cross sections on the same vertical scale, permitting comparison (at scattering angle 90°) of decay branching in the processes:

$$\mathrm{He}^-(1snln l',{}^2L)\rightarrow \mathrm{He}(1sn''s,{}^3S)+e^- \quad (3)$$

and

$$\rightarrow \mathrm{He}(1sn''s,{}^1S)+e^- \quad (4)$$

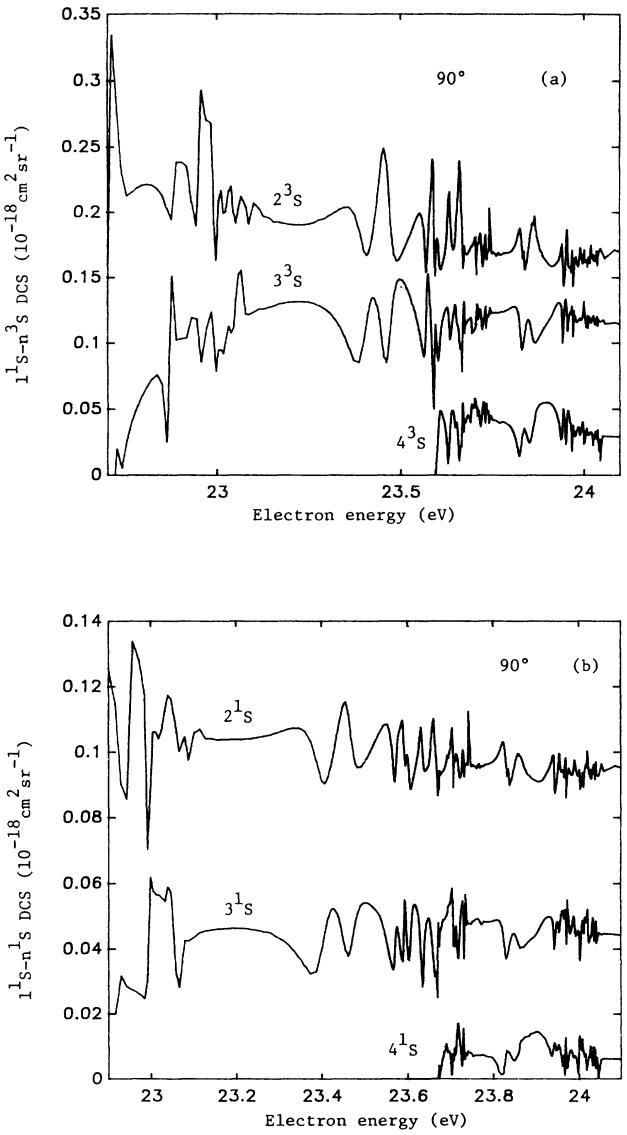

FIG. 7. The 29-state R-matrix calculations on the $1\,^1S-n\,^{3,1}S$ ($n=2$, 3, and 4) differential cross sections at scattering angle 90° shown on the same vertical scale facilitating comparison of the intensities of the sharp resonance features. (a) $1\,^1S-n\,^3S$ excitation; (b) $1\,^1S-n\,^1S$ excitation.

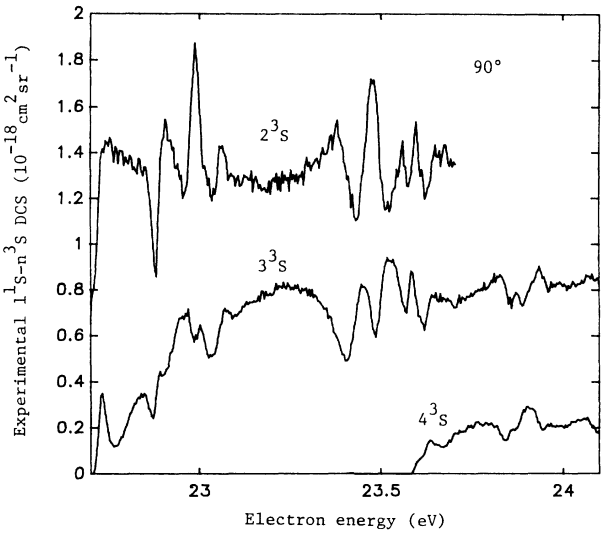

FIG. 8. Three experimental $n\,^3S$ cross sections, shown on the same vertical scale, facilitating comparison of the intensities of the sharp resonance features. From Allan [4].

for $n=3$ to 5 and $n''=2$ to 4. In comparison with Fig. 8, the present calculations [Fig. 7(a)] for the $1\,^1S-n\,^3S$ excitations, apart from having sharper structures, bear a remarkable resemblance to the experiments of Allan [4]. It is observed that the size of the resonant features for any given group of resonances n is about the same for all final channels n'', despite the substantial differences in magnitude between various $1\,^1S-n\,^3S$ excitation cross sections. Allan [4] interpreted this as uniform energy partition between the two electrons of a ridge state, with all the possible combinations of the bound- and free-electron energies having about equal weights. This behavior is recognized as resembling the nearly uniform energy partition between the two escaping electrons of a ridge state above the ionization threshold.

One important feature which was not reported by Allan [4] is that, if we are to compare Fig. 7(a) with Fig. 7(b), the resonant profiles for the singlet scattering $1\,^1S-n\,^1S$ lying just below the $n\,^3S$ ($n=3$, 4, and 5) threshold have structures identical to those in the triplet scattering $1\,^1S-n\,^3S$. The similarity in shape for these structures indicates that the doubly excited resonances $He^-(1sns^2,^2S^e)$, $He^-(1snsnp,^2P^o)$, and $He^-(1snsnd,^2D^e)$ decay uniformly into the $n\,^3S$ and $n\,^1S$ states.

Another interesting feature, reported by Allan on the shapes of the $He^-(1sns^2,^2S^e)$ resonant profiles (i.e., the lowest resonances connected with each n), emerges at any given scattering angle in the process:

$$He^-(1sns^2,^2S^e)\rightarrow He(1sn''s,^3S)+e^- . \quad (5)$$

The $He^-(1s4s^2,^2S^e)$ resonance at 23.43 eV appearing in the $2\,^3S$ cross section at 90° has a profile with a slow rise followed by a steep drop. The same profile is found for the $He^-(1s5s^2,^2S^e)$ resonance at 23.86 eV appearing in the $3\,^3S$ cross section. The same profile is also expected to be found for the $He^-(1sns^2,^2S^e)$ resonances appearing in the $n''\,^3S$ cross section for n'' ($=n-2$) taking the values 2,3,4,. . . [Fig. 7(a)]. In general, the profiles of the $He^-(1sns^2,^2S^e)$ resonances resemble each other while moving "diagonally" in Fig. 7(a), with the $He^-(1s4s^2,^2S^e)$ resonances appearing at the $2\,^3S$ excitation function as the first member of the pack, while both n and n'' are increased by 1. On the other hand, the profile of the $He^-(1s4s^2,^2S^e)$ at 23.43 eV appearing in the $3\,^3S$ cross section at 90° has a Fano profile (a slow drop followed by a steep rise of the cross section). The same Fano profile is found for $He^-(1s5s^2,^2S^e)$ resonance at 23.86 eV appearing in the $4\,^3S$ cross section. In general, the profiles of the $He^-(1sns^2,^2S^e)$ resonances appearing in the $n''\,^3S$ cross section resemble each other when n'' ($=n-1$), taking the values 2,3,4,. . . [see Fig.

7(a)], with the $He^-(1s3s^2,^2S^e)$ appearing in the $2\,^3S$ cross section as the leader of the pack. These two series move diagonally across Fig. 7(a) almost parallel to each other. The two series of profiles resemble each other, except that the sign of interference between the narrow resonant and broad underlying amplitude reverses. This interpretation of Allan [4] is clearly supported by our 29-state calculation on $1\,^1S-n\,^3S$ DCS [see Fig. 7(a)]. The same pattern holds for the $1\,^1S-n\,^1S$ excitations [see Fig. 7(b)].

In considering the change of l in the decay branching processes

$$He^-(1snsnp,^2P^o)\rightarrow He(1sn''l'',^3L)+e^- \quad (7)$$

Allan [4] suggested that a propensity rule $\Delta l=0$ holds for the above processes.

Figure 9 compares the $1\,^1S-2\,^{3,1}S$ and $1\,^1S-2\,^{3,1}P$ excitation functions as obtained from the 29-state R-matrix calculation by Fon, Lim, and Sawey [8,9]. The lowest resonance associated with $n=3$ threshold is $He^-(1s3s^2,^2S^e)$, which is prominent in the $2\,^3S$ and $2\,^1S$ excitation cross sections [see Figs. 9(a) and 9(b)] but virtually absent from the $2\,^3P$ cross section [see Fig. 9(c)]. While the resonance $He^-(1s3s3p,^2P^o)$ at 22.606 eV, the second lowest resonance of the $n=3$ group, appears to decay both into the $1s2s$ and the $1s2p$ final states in both cases, the propensity rule $\Delta l=0$ has not been violated (see Fig. 9). However, we are not fully convinced that the propensity rule $\Delta l=0$ holds in all cases. If we examine

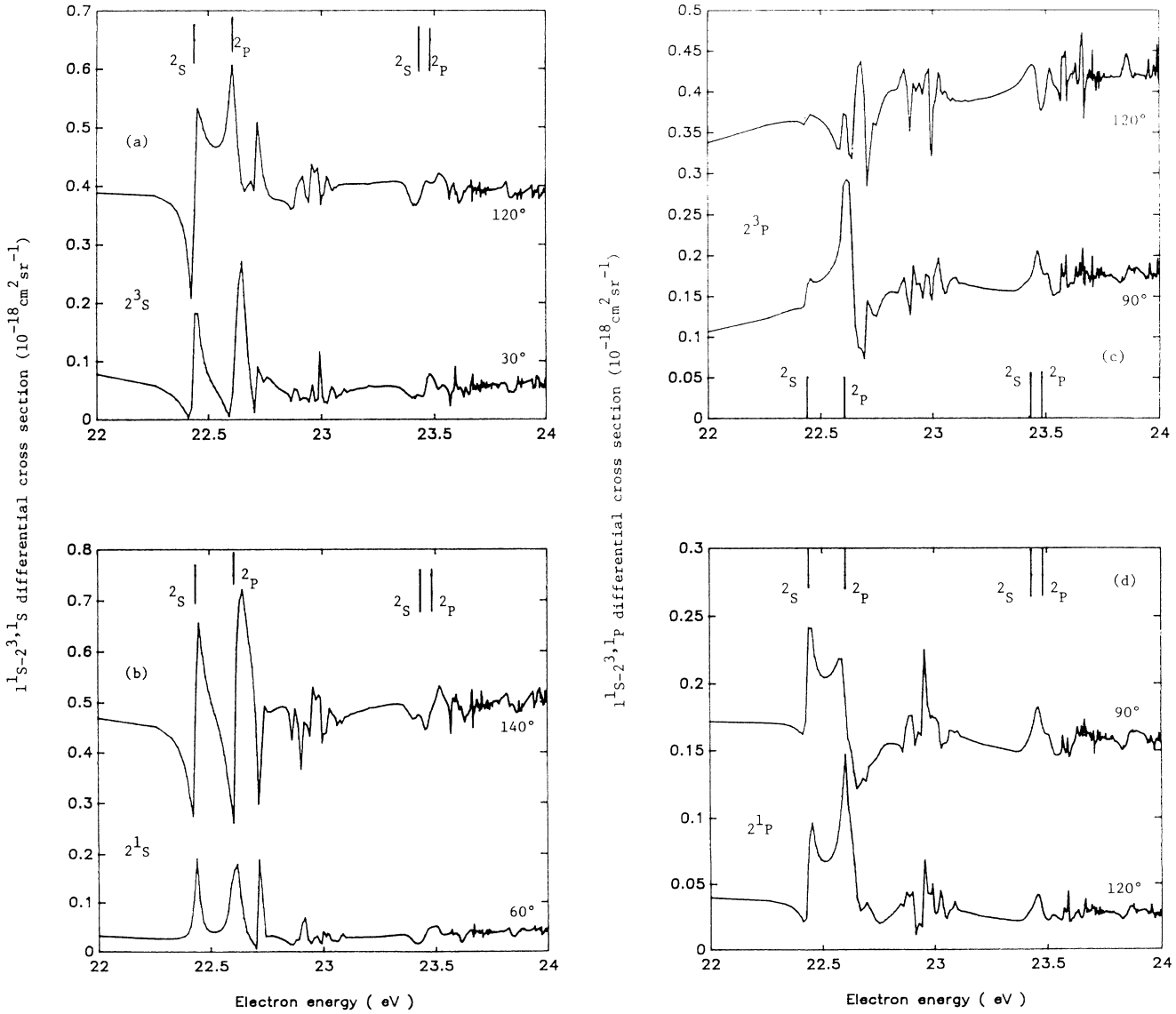

FIG. 9 The 29-state R-matrix calculations on $n=2$ inelastic differential cross sections (DCS) (10^{-18} cm^2 sr^{-1}). (a) $1\,^1S-2\,^3S$ DCS at scattering angles 30° and 120°; (b) $1\,^1S-2\,^1S$ DCS at scattering angles 60° and 140°; (c) $1\,^1S-2\,^3P$ DCS at scattering angles 90° and 120°; (d) $1\,^1S-2\,^1P$ DCS at scattering angles 90° and 120°. The upper curves in (a)–(d) are shown as vertical offsets.

the case of the lowest resonances $He^-(1s3s^2,^2S^e)$ and $He^-(1s3s3p,^2P^o)$ associated with the $n=3$ group of resonances which decay into the $2\,^1P$ final state, both resonances are prominently indicated at 22.435 and 22.606 eV. The propensity rule has been violated. Again, if we look at the decay of the two lowest resonances $He^-(1s4s^2,^2S^e)$ and $He^-(1s4s4p,^2P^o)$ associated with $n=4$ group, the two resonances overlap and form a prominent peak in the $2\,^1P$ cross section. In this case, it is very hard for us to form an opinion on the propensity rule.

It is very difficult to describe $1\,^1S-n\,^{3,1}P$ excitation. This is due to the fact that the partial waves with $L>0$ are split into two channels corresponding to outgoing angular momenta $l=L+1$ and $l=L-1$ in the S-P transitions; in addition, different angular dependences are associated with the excitation of the $m=0$ and $m=\pm 1$ substates. For the same reason, the $1\,^1S-2\,^1P$ excitation functions were not used to identify resonances by Fon and Lim [17].

IV. CONCLUSION

We have carried out the 19-state and 29-state R-matrix calculations for $1\,^1S-n\,^3S$ ($n=3$ and 4) excitation cross sections, and convergences between the R-matrix calculations has been established (see also [14]). Comparison between the 29-state calculations and the experiments [4] shows excellent qualitative agreement. The results, together with those of Fon, Lim, and Sawey [8,9] for $n=2$ excitations, show that the observation of Allan [4] on the uniform energy partition between the two electrons of a doubly excited Wannier-ridge state is essentially correct. The only plausible explanation for this phenomenon is that the electron-electron correlation and interchannel coupling are so strong as to give rise to formation of a highly symmetrical localized electron-density distribution along the Wannier ridge. However, the present calculation does not seem to support the propensity rule $\Delta l=0$ for the decay of doubly excited Wannier-ridge resonances as proposed by Allan [4]. Further theoretical and experimental investigations are needed.

ACKNOWLEDGMENTS

We would like to thank Professor P. G. Burke and Professor A. E. Kingston and Dr. K. A. Berrington from Queen's University of Belfast, Northern Ireland, for helpful discussions and their continued interest in this project. We wish to thank Professor M. Allan from Universitäta Freiburg Schweiz for sending us his latest experimental data. The computing was carried out on the Cray X-Mp/48 computer at the Atlas Supercomputer Centre, the Rutherford Appleton Laboratory, Didcot, UK. Data analysis was carried out on the UNISYS 1100/61 computer system at the Computer Centre, University of Malaya, Kuala Lumpur, Malaysia.

[1] G. H. Wannier, Phys. Rev. **90**, 817 (1953).
[2] I. Vinkalus and M. Gailitis, in *Proceedings of the Fifth International Conference on the Physics of Electronic and Atomic Collisions, Leningrad, 1967,* edited by I. P. Flaks (Nauka, Leningrad, 1967), p. 648.
[3] S. Cvejanovic and F. H. Read, J. Phys. B **7**, 1841 (1974).
[4] M. Allan, J. Phys. B **25**, 1559 (1992).
[5] F. Pichou, A. Huetz, G. Joyez, M. Landau, and J. Mazeau, J. Phys. B **9**, 993 (1976).
[6] K. A. Berrington and A. E. Kingston, J. Phys. B **20**, 6631 (1987).
[7] P. M. J. Sawey, K. A. Berrington, P. G. Burke, and A. E. Kingston, J. Phys. B **23**, 4321 (1990).
[8] W. C. Fon, K. P. Lim, and P. M. J. Sawey, J. Phys. B **26**, 305 (1993).
[9] W. C. Fon, K. P. Lim, and P. M. J. Sawey, J. Phys. B **26**, 4201 (1993).
[10] P. G. Burke, A. Hibbert, and W. D. Robb, J. Phys. B **4**, 153 (1971).
[11] K. A. Berrington, P. G. Burke, M. Le Dourneuf, W. D. Robb, K. T. Taylor, and Vo Ky Lan, Comput. Phys. Commun. **14**, 367 (1978).
[12] The results can be obtained in printed form or via electronic mail at the address j2wcfon@fileserver.ce.um.My
[13] W. C. Martin, J. Phys. Chem. Ref. Data **2**, 257 (1973).
[14] W. C. Fon, K. Ratnavelu, and P. M. J. Sawey, J. Phys. B **26**, L555 (1993).
[15] W. C. Fon and K. P. Lim, J. Phys. B **23**, 3691 (1990).
[16] W. C. Fon and K. P. Lim, J. Phys. B **25**, 3513 (1992).
[17] W. C. Fon and K. P. Lim, J. Phys. B **26**, 2717 (1993).
[18] J. M. Phillips and S. F. Wong, Phys. Rev. A **23**, 3324 (1981).
[19] D. Andrick, J. Phys. B **12**, L175 (1979).
[20] W. C. Fon, K. A. Berrington, P. G. Burke, and A. E. Kingston, J. Phys. B **22**, 3939 (1989).